Progress In Electromagnetics Research, Vol. 138, 421–432, 2013

GIANT CIRCULAR DICHROISM AND NEGATIVE REFRACTIVE INDEX OF CHIRAL METAMATERIAL BASED ON SPLIT-RING RESONATORS

Yongzhi Cheng, Yan Nie, Lin Wu, and Rongzhou Gong*

School of Optical and Electronic Information, Huazhong University of Science and Technology, Wuhan 430074, China

Abstract—In this paper, a double-layer split-ring resonator structure chiral metamaterial was proposed which could exhibit pronounced circular dichroism (CD) effect and negative refractive index at microwave frequencies. Experiment and simulation calculations are in good agreement. The retrieved effective electromagnetic parameters indicate that the lower frequency CD effect is associated with the negative refractive index property of the left circularly polarized (LCP) wave, and the upper one is to the right circularly polarized (RCP) wave. The mechanism of the giant CD effect could be further illustrated by simulated surface current and power loss density distributions.

1. INTRODUCTION

Electromagnetic (EM) metamaterials (MMs) is a new class of artificial materials possessing exotic properties and capability for the manipulations of the behaviors of the incident EM or light wave radiation that are not found in nature [1]. MMs have become an excellent platform for some unique applications, such as superlens, cloaking, electric devices, and so on [2–5]. Recently, more and more interest has been focused on the chiral metamaterial (CMM) structures due to their attractive EM (optical) properties such as strong optical activity, circular dichroism (CD) and negative refractive index (NRI) from microwave to optical range [6–22]. Intuitively, CMMs cannot be brought into congruence with their mirror images (the so-called enantiomer), which neither violates reciprocity nor time-reversal symmetry. This kind of configuration can make electric and magnetic dipoles excited along the same direction driven by electric or magnetic

Received 12 January 2013, Accepted 26 February 2013, Scheduled 28 March 2013

* Corresponding author: Rongzhou Gong (rzhgong@mail.hust.edu.cn).

field of incident EM wave [12–16]. Optical activity is well-known as optical polarization rotation, which could rotate the polarization plane of a linearly polarized wave, and described as polarization azimuth rotation angle $\theta = [\arg(T_{++}) - \arg(T_{--})]/2$ [23], where the T_{++} and T_{--} is transmitted coefficients of the right circularly polarized (RCP, $++$) waves and left circularly polarized (LCP, $--$) waves, respectively. Similar to the optical activity, another important property is CD ($\Delta = |T_{++}| - |T_{--}|$) effect, which can form the transmission intensity difference between the RCP waves and the LCP waves due to different absorption for each handedness. The last is the ellipticity expressed as $\eta = \arctan[(|T_{++}| - |T_{--}|)/(|T_{++}| + |T_{--}|)$, which defines the difference of polarization state of transmitted and incident waves, and also measures the CD effect.

More recently, the CD effect has gained a lot of attentions due to its wide applications in photonic crystals, quantum devices, optical communication, sensing, imaging, and high density data storage [24, 25]. Although the CD phenomenon also can be observed in planar as well as double-layered non-chiral MMs structures [24–29], it is usually very small ($|\Delta| < 0.4$) and required an oblique incident wave. It is expected that 3D or 2D CMMs, like multilayered helical or double-layer gammadion structures, are likely to exhibit CD effect and/or large optical activity. Therefore, CMM would be a good candidate to achieve a large CD effect. However, the previous designs of chiral structures are mainly focused on the giant optical activity as well as NRI properties, and usually neglect the CD effect. On the other hand, these designed chiral structures may exhibit very small CD effect.

In this work, we designed a novel CMM using double-layer SRRs structure assembly of mutually twisted planar metal patterns in parallel planes. The microwave experiment and simulation results of the proposed chiral structure exhibit giant CD effect. The experimental results are in good agreement with the numerical simulation. Effective parameters of this structure, such as refractive index, chirality parameter, permeability and permittivity are retrieved from simulated transmissions and refiections. The mechanism of the giant CD effect also could be further illustrated by simulated surface current and power loss density distributions.

2. PHYSICAL MODEL, SIMULATION AND EXPERIMENT

Since the beginning of the proposal of MMs, SRR has played an important role in achieving negative permeability, negative refractive index, coupling effect and other exotic phenomena [30–39]. The two

mutually twisted SRRs also can be formed a magnetic dimer possessing optical activity [39]. So, it also inspires us to construct a CMM with giant CD effect and NRI properties using SRR structures assembly.

Here, our designed CMM is composed of a two-dimensional periodic array of SRR copper foils assembly separated by a dielectric slab, in which the SRR pairs are arranged in C4 symmetry and the unit cell is shown in Figure 1(a). Thus, the overall unit structure has uniaxial fourfold rotational symmetry for the normal incidence wave direction, not any mirror plane and center of inversion. The geometry dimension parameters are as follow: $p = 13.6\,\text{mm}$, $r_1 = 2.8\,\text{mm}$, $r_2 = 1.2\,\text{mm}$, $g = 0.5\,\text{mm}$, $t_s = 1\,\text{mm}$. The metallic SRRs layers in both sides were modeled as a 0.036 mm copper film with an electric conductivity $\sigma = 5.8 \times 10^7\,\text{S/m}$. The FR-4 (lossy) substrate with a permittivity of 4.2 and a loss tangent of 0.025 was selected as the middle dielectric spacer [19].

The numerical simulations were performed based on the standard finite difference time domain (FDTD) by using the frequency domain solver of the CST Microwave Studio. The periodic boundary conditions were applied to the x and y directions and the absorbing boundary conditions were applied to the z direction. For experiments, the designed structures are fabricated into a 29×29 unit cell sample ($400\,\text{mm} \times 400\,\text{mm} \times 1.072\,\text{mm}$) by the conventional printed circuit board (PCB) process, and the photograph of portion of a fabricated CMM sample is shown in Figure 1(b). Agilent PNA-X N5244A vector network analyzer connected to the two standard gain broadband linearly polarized horn antennae that produced microwaves in the range of 4–9 GHz were employed to measure the CMM sample in

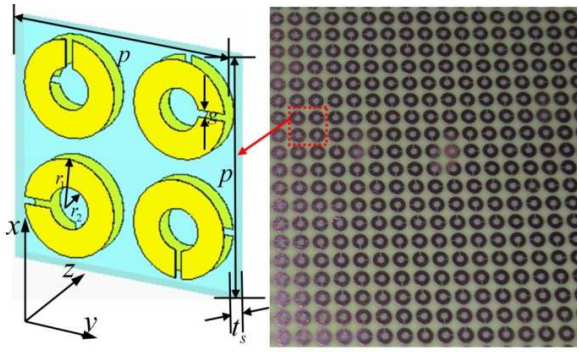

Figure 1. Schematics of designed unit-cell CMM structure: (a) perspective view of the unit cell structure, (b) portion photography of the tested sample.

an EM anechoic chamber [40, 41], finally, we can obtain the complex transmission. A linearly polarized EM wave (**E** field in the x) direction is incident on the CMM structure sample. On the other side of the sample, we measured the transmitted coefficients (T_{xx} and T_{yx}) in the x and y polarizations. In our designed CMM structure, circular polarization conversion is absent due to the fourfold rotational symmetry. Assuming the electric field of the incident linearly polarized wave is along x direction, the electric field of the transmitted wave can be stated as $\mathbf{E}_{\pm} = \mathbf{E}_0(T_{xx}\hat{x} \pm T_{yx}i\hat{y})$ [23]. Thus, the RCP and LCP transmitted coefficients (T_{++} and T_{--}) can be calculated from the linear transmitted coefficients (T_{xx} and T_{yx}) with $T_{++/--} = T_{xx} \pm iT_{yx}$ [10–16].

3. RESULTS AND DISCUSSION

Figures 2(a) and (b) show the simulation (a) and experimental (b) results of transmission spectra (T_{++}/T_{--}) for the RCP and LCP waves. There are significant differences between the transmission of

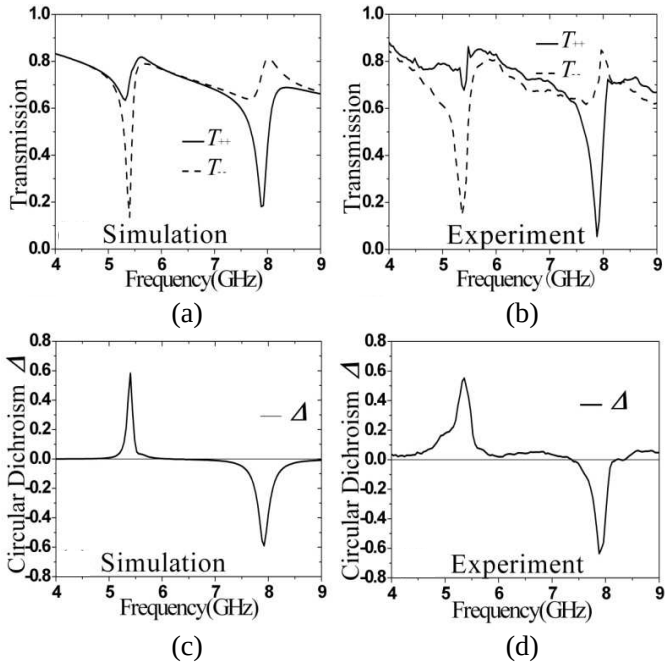

Figure 2. Simulation and experiment results for the CMM: (a) and (b) are the transmission spectra for RCP and LCP waves, (c) and (d) are the CD spectra.

RCP and LCP waves around the resonances, which is due to the asymmetric geometry along the propagating direction. It can be seen that the transmission of RCP wave is 0.5–0.6 higher than that of the LCP wave around 5.4 GHz, while the transmission of the RCP wave is 0.5–0.6 lower than that of the LCP wave around 7.9 GHz. It means that the LCP waves at lower frequency resonance and RCP waves at higher frequency resonance are forbidden to transmit mostly, respectively. Figures 2(c) and (d) present the simulation and experiment CD spectra for the structure. The main CD peaks can be observed around the resonances, and the maximal value (absolute value) is up to 0.58, which is much greater than the current reported chiral and non-chiral structures [6–17, 19–22, 24–29]. From the CD spectra, we can conclude that the designed structure can absorb strongly LCP wave at lower frequency resonance (around 5.4 GHz) and RCP wave at higher frequency resonance (around 7.9 GHz), respectively.

In Figure 3, we show the simulation (a) and experiment (b) results of polarization azimuth rotation angle θ and ellipticity η of the transmitted wave. The θ and η reach their maximum values, ($\theta = -53.6°$, $\eta = 34°$) and ($\theta = 218.4°$, $\eta = 31.2°$) at the resonance frequencies of 5.4 GHz and 7.9 GHz for simulation, respectively. It can also be seen clearly that the η is near zero ($\eta \approx 0$) in a broadband frequency range (from 5.6 GHz to 7.4 GHz), where is corresponding to a pure optical activity effect. It's mean that the CMM can rotate a incident linearly polarized wave a certain angle θ at this frequency range, and the transmitted wave is still linear polarization. The average rotation angle θ is about 11° for 1.072-mm-thick MM when $\eta \approx 0$, obviously, which is relative smaller comparing with the previous CMM

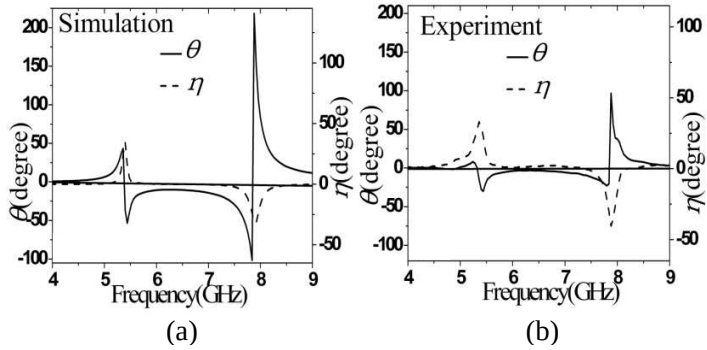

Figure 3. The polarization azimuth rotation angle (θ) and ellipticity (η): (a) simulation, (b) experiment.

structures [6–17, 19–21].

A standard parameter retrieval method was used to calculate the effective EM parameters of the proposed CMMs [11]. Here, the retrieved real parts of effective EM parameters can be obtained based on the simulation data of the transmission and refiection for one layer of the CMM. The real parts of the permittivity (ε) and the permeability (μ) as a function of frequency for the asymmetric SRR pairs assembly are shown in Figure 4(a). Obviously, the Re(μ) is near unity throughout the entire frequency range except the tiny range at 7.9 GHz (around this frequency, the Re(μ) is negative). While two significant resonance dips can be observed for Re(ε), and the Re(ε) is also negative around 7.9 GHz. There is overlap region of negative ε and μ, which is conspicuous different to the previous designed CMM structures [10–16].

In Figure 4(b), we also show the real part of the effective refractive index (n, n_+, n_-) and chiral parameter (κ). There are two resonances related to the chirality for the κ curves. The lower frequency resonance happens at 5.4 GHz, and the upper one happens at 7.9 GHz. It can be observed that the n is negative around the 7.9 GHz, which is similar to the traditional NRI MMs required simultaneous negative ε and μ ($n = \sqrt{\varepsilon\mu}$). The κ is always negative when frequency is above 7.9 GHz and below 5.4 GHz, and the negative maximal value ($\kappa = -3.6$) also can be obtained around the upper frequency. Due to the relation of $n_\pm = n \pm \kappa$, the strong chirality has pushed the refractive index of the LCP wave from positive to negative values above 5.4 GHz, and the

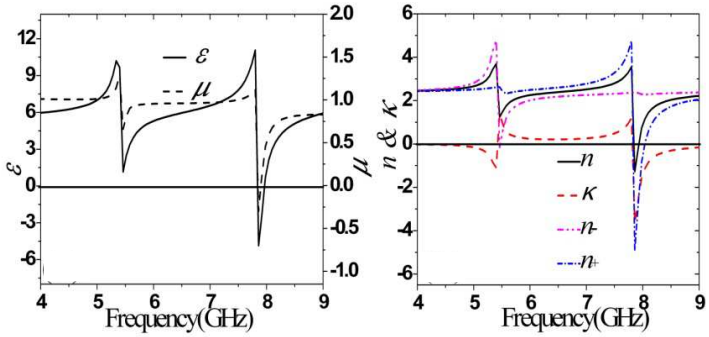

Figure 4. The extracted effective parameters from the simulation data: (a) the real part of the effective permittivity (ε) and permeability (μ), (b) the real part of the effective refractive index (n, n_+, n_-) and chiral parameter (κ).

refractive index of the RCP wave from positive to negative values below 7.9 GHz, respectively. Thus, we can conclude that the lower frequency giant CD effect is associated with the NRI property of the LCP wave, and the upper one is associated with the NRI property of the RCP wave.

In order to better understand the mechanism of the giant CD effect for the designed CMM structure, we studied the surface current and power loss density distributions driven by the incident field with **E** in the x direction at 5.4 GHz and 7.9 GHz, as shown in Figures 5 and 6, respectively. From Figure 5(a), the currents on the front and back four SRRs are in the same direction at 5.4 GHz, which is a symmetric resonance mode as coupled electric dipoles resonance. On the contrary, as shown in Figure 5(b), the currents on the front and back four SRRs are in the opposite directions at 7.9 GHz, which is corresponding to an asymmetric resonance mode as coupled magnetic dipoles resonance. On the other hand, as shown in Figure 5(c), the x component of electric field of the second interface is along $-x$ direction and the y

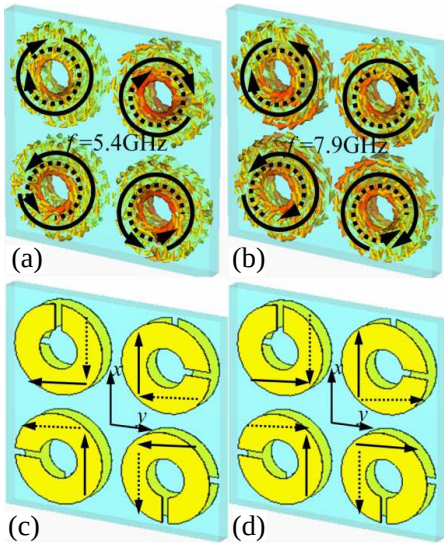

Figure 5. (a) and (b) indicate the surface current distribution when driven by the incident field with **E** in the x direction at 5.4 GHz and 7.9 GHz, respectively. (c) and (d) indicate the schematics of the induced electric field direction when driven by the incident field with **E** in the x direction at 5.4 GHz and 7.9 GHz, respectively. The solid (dashed) line arrows represent the front (back) surface current distribution and induced electric field direction.

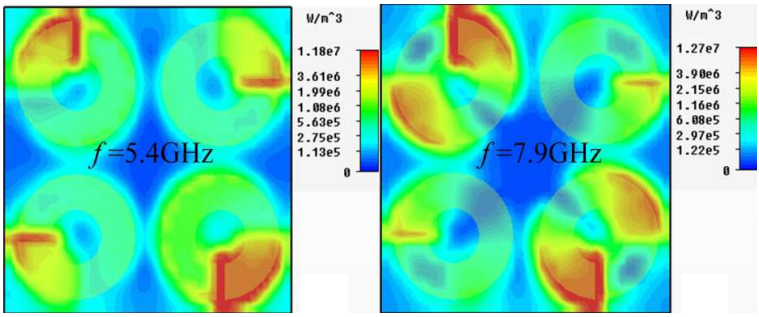

Figure 6. The power loss density distribution in the middle of the SRR pairs when driven by the incident field with **E** in the x direction at (a) 5.4 GHz and (b) 7.9 GHz.

component is along $-y$ direction at 5.4 GHz, which illustrates that a RCP wave is achieved. However, as shown in Figure 5(d), at 7.9 GHz, the x component of electric field of the second interface is along $-x$ direction and the y component is along $+y$ direction, which indicates that a LCP wave is realized. Thus, the surface current distributions indicate that the excitation of giant CD effect of the lower frequency is mainly due to the local electric dipoles resonance, and the one of the higher frequency is mainly from the local magnetic dipoles resonance.

Figure 6 shows the power loss density distribution in the middle of the SRR pairs when driven by the incident field with **E** in the x direction at 5.4 GHz (a) and 7.9 GHz (b). Obviously, at the lower frequency (5.4 GHz), the power loss is mainly focused on a single region for each different SRR pair, which indicates the typical local electric dipoles resonance. While the power loss is mainly concentrated on a double region for each different SRR pair at the higher frequency (7.9 GHz), which indicates the typical local magnetic dipoles resonance. The power loss density distributions confirm that the CD observed in the experiment and simulation for the proposed CMM results from the difference in the losses in the metal due to the current induced by the incidence wave.

4. CONCLUSION

In conclusion, we propose a CMM composed of four twisted SRR structure, which could exhibit giant CD effect and NRI properties at microwave frequencies. Both simulation and experiment exhibit that the maximal value (absolute value) of CD is up to 0.58 at resonances,

which is much greater than the current reported chiral and non-chiral structures [6–17, 19–22, 24–29]. The retrieved effective EM parameters indicate that the lower frequency CD effect is associated with the NRI property of the LCP wave, and the upper one is to the RCP wave. The mechanism of the giant CD effect also could be further illustrated by simulated surface current and power loss density distributions. The generation mechanism of giant CD effect of the lower frequency is mainly due to the local electric dipoles resonance, and the one of the higher frequency is mainly from the local magnetic dipoles resonance. In addition, if the dimensions of the proposed CMM structure are reduced to micro-, nano- and even lower scale, the giant CD effect and NRI properties could also be operated to function at other frequency bands, such as millimeter wave, terahertz, or even optical range. The proposed CMM structure could also be beneficial in designing optical functional materials, such as waveplates and circular polarizers.

REFERENCES

1. Veselago, V. G., "The electrodynamics of substances with simultaneously negative values of ε and μ," *Sov. Phys. Usp.*, Vol. 10, No. 4, 509–514, 1968.
2. Pendry, J. B., "Negative refraction makes a perfect lens," *Phys. Rev. Lett.*, Vol. 85, No. 18, 3966–3969, 2000.
3. Schurig, D., J. J. Mock, B. J. Justice, S. A. Cummer, J. B. Pendry, A. F. Starr, and D. R. Smith, "Metamaterial electromagnetic cloak at microwave frequencies," *Science*, Vol. 314, No. 5801, 977–980, 2006.
4. Kasabegoudar, V. G. and K. J. Vinoy, "A broadband suspended microstrip antenna for circular polarization," *Progress In Electromagnetics Research*, Vol. 90, 353–368, 2009.
5. Shi, Y., "A compact polarization beam splitter based on a multimode photonic crystal waveguide with an internal photonic crystal section," *Progress In Electromagnetics Research*, Vol. 103, 393–401, 2010.
6. Rogacheva, A. V., V. A. Fedotov, A. S. Schwanecke, and N. I. Zheludev, "Giant gyrotropy due to electromagnetic-field coupling in a bilayered chiral structure," *Phys. Rev. Lett.*, Vol. 97, No. 17, 177401, 2006.
7. Dong, J., "Exotic characteristics of power propagation in the chiral nihility fiber," *Progress In Electromagnetics Research*, Vol. 99, 163–178, 2009.
8. Dong, J., "Surface wave modes in chiral negative refraction

grounded slab waveguides," *Progress In Electromagnetics Research*, Vol. 95, 153–166, 2009.

9. Dong, J. F., J. Li, and F.-Q. Yang, "Guided modes in the four-layer slab waveguide containing chiral nihility core," *Progress In Electromagnetics Research*, Vol. 112, 241–255, 2011.
10. Plum, E., J. Zhou, J. Dong, V. A. Fedotov, T. Koschny, C. M. Soukoulis, and N. I. Zheludev, "Metamaterial with negative index due to chirality," *Phys. Rev. B*, Vol. 79, No. 3, 035407(6), 2009.
11. Zhou, J., J. Dong, B. Wang, T. Koschny, M. Kafesaki, and C. M. Soukoulis, "Negative refractive index due to chirality," *Phys. Rev. B*, Vol. 79, No. 12, 121104(4), 2009.
12. Wu, Z., B. Q. Zhang, and S. Zhong, "A double-layer chiral metamaterial with negative index," *Journal of Electromagnetic Waves and Applications*, Vol. 24, No. 7, 983–992, 2010.
13. Li, Z., R. Zhao, T. Koschny, M. Kafesaki, K. B. Alici, E. Colak, H. Caglayan, E. Ozbay, and C. M. Soukoulis, "Chiral metamaterials with negative refractive index based on four "U" split ring resonators," *Appl. Phys. Lett.*, Vol. 97, No. 8, 081901(3), 2010.
14. Decker, M. R. Z., C. M. Soukoulis, S. Linden, and M. Wegener, "Twisted split-ring-resonator photonic metamaterial with huge optical activity," *Opt. Lett.*, Vol. 35, No. 10, 1593–1593, 2010.
15. Li, J., F. Q. Yang, and J. F. Dong, "Design and simulation of L-shaped chiral negative refractive index structure," *Progress In Electromagnetics Research*, Vol. 116, 395–408, 2011.
16. Zarifi, D., M. Soleimani, and V. Nayyeri, "A novel dual-band chiral metamaterial structure with giant optical activity and negative refractive index," *Journal of Electromagnetic Waves and Applications*, Vol. 26, Nos. 2–3, 251–263, 2012.
17. Zhao, R., L. Zhang, J. Zhou, T. Koschny, and C. M. Soukoulis, "Conjugated gammadion chiral metamaterial with uniaxial optical activity and negative refractive index," *Phys. Rev. B*, Vol. 83, No. 3, 035105(4), 2011.
18. Canto, J. R., C. R. Paiva, and A. M. Barbosa, "Dispersion and losses in surface waveguides containing double negative or chiral metamaterials," *Progress In Electromagnetics Research*, Vol. 116, 409–423, 2011.
19. Cheng, Y. Z., Y. Nie, and R. Z. Gong, "Giant optical activity and negative refractive index using complementary U-shaped structure assembly," *Progress In Electromagnetics Research M*, Vol. 25, 239–

253, 2012.

20. Li, Z., K. B. Alici, H. Caglayan, M. Kafesaki, C. M. Soukoulis, and E. Ozbay, "Composite chiral metamaterials with negative refractive index and high values of the figure of merit," *Opt. Express*, Vol. 20, No. 16, 6146–6156, 2012.
21. Sabah, C. and H. G. Roskos, "Design of a terahertz polarization rotator based on a periodic sequence of chiral-metamaterial and dielectric slabs," *Progress In Electromagnetics Research*, Vol. 124, 301–314, 2012.
22. Zarifi, D., H. Oraizi, and M. Soleimani, "Improved performance of circularly polarized antenna using semi-planar chiral metamaterial covers," *Progress In Electromagnetics Research*, Vol. 123, 337–354, 2012.
23. Jackson, J. D., *Classical Electrodynamics,* 3rd Edition, 205–207, Wiley, 1999.
24. Decker, M., M. W. Klein, M. Wegener, and S. Linden, "Circular dichroism of planar chiral magnetic metamaterials," *Opt. Lett.*, Vol. 32, No. 7, 856–858, 2007.
25. Plum, E., X. X. Liu, V. A. Fedotov, Y. Chen, D. P. Tsai, and N. I. Zheludev, "Metamaterials: Optical activity without chirality," *Phys. Rev. Lett.*, Vol. 102, No. 11, 113902-4, 2009.
26. Yannopapas, V., "Circular dichroism in planar nonchiral plasmonic metamaterials," *Opt. Lett.*, Vol. 34, No. 5, 632–634, 2009.
27. Gao, W., H. M. Leung, Y. Li, H. Chen, and W. Y. Tam, "Circular dichroism in double layer metallic crossed-gratings," *J. Opt.*, Vol. 13, No. 11, 115101-8, 2011.
28. Feng, C., Z. B. Wang, S. Lee, J. Jiao, and L. Li, "Giant circular dichroism in extrinsic chiral metamaterials excited by off-normal incident laser beams," *Opt. Communications*, Vol. 285, 2750–2754, 2012.
29. Cao, T. and M. J. Cryan, "Circular dichroism in planar nonchiral metamaterial made of elliptical nanoholes array," *Journal of Electromagnetic Waves and Applications*, Vol. 26, No. 10, 1275–1282, 2012.
30. Wongkasem, N., A. Akyurtlu, J. Li, A. Tibolt, Z. Kang, and W. D. Goodhue, "Novel broadband terahertz negative refractive index metamaterials: Analysis and experiment," *Progress In Electromagnetics Research*, Vol. 64, 205–218, 2006.
31. Andres-Garcia, B., L. E. Garcia-Munoz, V. Gonzalez-Posadas, F. J. Herraiz-Martinez, and D. Segovia-Vargas, "Filtering lens

structure based on SRRs in the low THz band," *Progress In Electromagnetics Research*, Vol. 93, 71–90, 2009.

32. Cheng, Y. Z., H. L. Yang, Y. Nie, R. Z. Gong and Z. Z. Cheng, "Investigation of negative index properties of planar metamaterials based on split-ring pairs," *Appl. Phys., A Mater. Sci. Process.*, Vol.103, No. 4, 989–994, 2011.
33. Aznabet, M., M. Navarro-Cia, M. Beruete, F. J. Falcone, M. Sorolla Ayza, O. El Mrabet, and M. Essaaidi, "Transmission properties of stacked SRR metasurfaces in free space," *Progress In Electromagnetics Research M*, Vol. 20, 1–11, 2011.
34. Carbonell, J., E. Lheurette, and D. Lippens, "From rejection to transmission with stacked arrays of split ring resonators," *Progress In Electromagnetics Research*, Vol. 112, 215–224, 2011.
35. Nornikman, H., B. H. Ahmad, M. Z. A. Abdul Aziz, M. F. B. A. Malek, H. Imran, and A. R. Othman, "Study and simulation of an edge couple split ring resonator (EC-SRR) on truncated pyramidal microwave absorber," *Progress In Electromagnetics Research*, Vol. 127, 319–334, 2012.
36. Zhang, F., Q. Zhao, J. Sun, J. Zhou, and D. Lippens, "Coupling effect of split ring resonator and its mirror image," *Progress In Electromagnetics Research*, Vol. 124, 233–247, 2012.
37. Rigi-Tamandani, A., J. Ahmadi-Shokouh, and S. Tavakoli, "Wideband planar split ring resonator based metamaterials," *Progress In Electromagnetics Research M*, Vol. 28, 115–128, 2013.
38. Guo, W., L. He, B. Li, T. Teng, and X. W. Sun, "A wideband and dual-resonant terahertz metamaterial using a modified SRR structure," *Progress In Electromagnetics Research*, Vol. 134, 289–299, 2013.
39. Liu, H., D. A. Genov, D. M. Wu, Y. M. Liu, Z. W. Liu, C. Sun, S. N. Zhu, and X. Zhang, "Magnetic plasmon hybridization and optical activity at optical frequencies in metallic nanostructures," *Phys. Rev. B*, Vol. 76, 073101, 2007.
40. Cheng, Y. Z. and H. L. Yang, "Design, simulation, and measurement of metamaterial absorber," *J. Appl. Phys.*, Vol. 108, No. 3, 034906(4), 2010.
41. Song, K., X. P. Zhao, Q. H. Fu, Y. H. Liu, and W. R. Zhu, "Wide-angle 90°-polarization rotator using chiral metamaterial with negative refractive index," *Journal of Electromagnetic Waves and Applications*, Vol. 26, Nos. 14–15, 1967–1976, 2012.